A Novel Electronically Controllable of Current-Mode Level Shifted Multicarrier PWM Based on MO-CFTA

Weerapon KONGNUN, Apinan AURASOPON

Department of Electrical Engineering, Mahasarakham University, Mahasarakham, Thailand

weerapon.kong@gmail.com, apinan.a@msu.ac.th

Abstract. *This paper proposes the application of an electronically controlled current-mode for a level shifted multicarrier PWM generator. The proposed circuit consists of two multiple-output current follower transconductance amplifiers (MO-CFTAs) for the multiple-output triangular generator and four current follower transconductance amplifiers (CFTAs) for the signal comparator. The characteristics of the circuit are as follows: the current output can be controlled by bias current, the maximum amplitude deviation due to temperature variation is less than 1.37 % and the power consumption is approximately 0.744 μW, at ±1.5 V supply voltages. The proposed PWM has been verified through PSpice simulation results which are in consistent with the theoretical analysis.*

Keywords

Current-mode, level shifted multicarrier PWM, MO-CFTA.

1. Introduction

Multilevel voltage source inverters have been widely used for high power applications such as water pumping stations, exhaust gas fans, induction motor controller, reactive power compensation, grid integration of renewable energy, and more different applications [1]-[8]. This is because they have many advantages such as low power dissipation on power switches, low harmonic contents and low electromagnetic interference (EMI) outputs.

Fig. 1 shows a classification of the multilevel voltage source inverter topologies that is divided at two groups: single and multiple DC source topologies. These topologies consist of many switches for generating the multilevel output voltage. To control the operation of these switches, the general basic pulse-width modulation (PWM) such as sinusoidal PWM or space vector PWM cannot be directly used. Thus, the complex PWM techniques have been used and can be divided at two groups: low and high switching frequency techniques as shown in Fig. 2. Generally, the switching loss and the percentage of total harmonic distortion (THD) are used for selecting the modulation strategies [9]. However, in some applications, the simple modulation strategies are required. The simple modulation techniques for the multilevel voltage source inverters are the multicarrier PWM technique which has two groups: In the phase shifted PWM, the phase difference of triangular carriers is used in modulation process. While the level shifted PWM the amplitude difference of triangular carriers is used. However, the most popular and simple switching scheme for controlling the multilevel voltage source inverters is level shifted PWM [10].

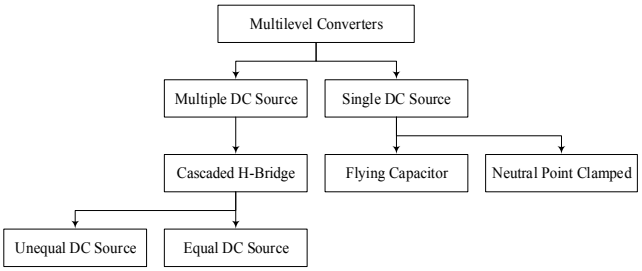

Fig. 1. A classification of the multilevel converters.

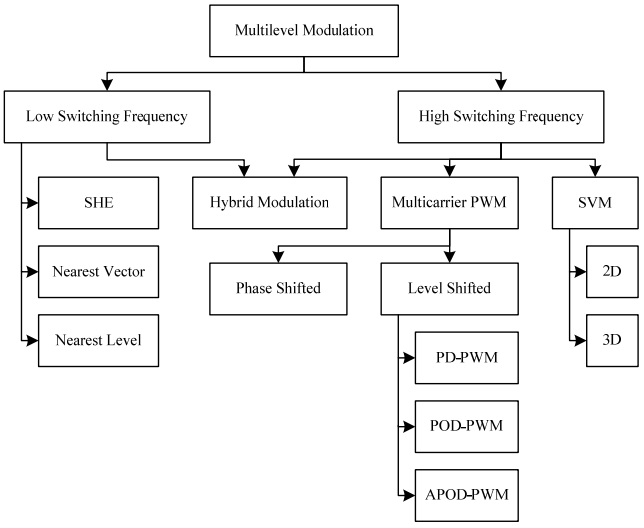

Fig. 2. A classification of the multilevel modulation topologies.

The level shifted multicarrier PWM can be distinguished in three methods: Phase Disposition (PD), Phase Opposition Disposition (POD) and Alternative Phase Opposition Disposition (APOD) as shown in Fig. 3. The PD method gives the lowest harmonic distortion at high modulation indices when compared to the other methods [11], [12]. Moreover, this method is an optimal solution

when used in carrier-based space-vector PWM for three-phase inverter [13]. However, in this paper, all methods will be examined in simulation results.

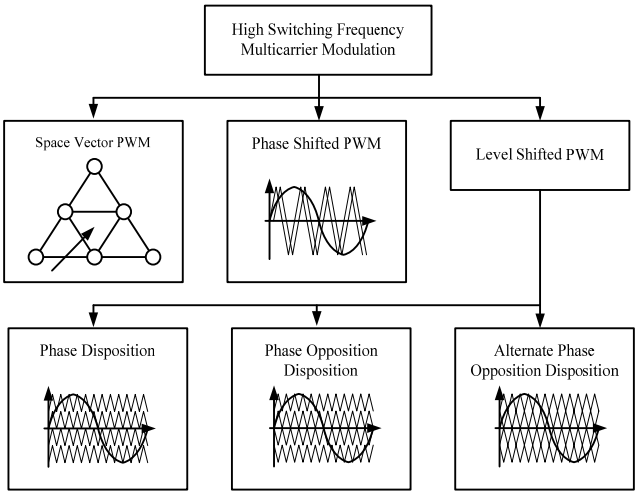

Fig. 3. Three basics of the multicarrier modulation topologies.

In recent year, most of analog circuit design uses a current-mode technique because this technique has more potential advantages such as wide bandwidth, large dynamic range, simple circuit and good linearity [14-21]. The mix-mode device current follower transconductance amplifier (CFTA) proposed in 2011 [22] is very suitable for the design and synthesis analog circuit and signal processing, and its transconductance gain can be controlled by the corresponding bias current. Moreover, using CFTA as an active element is more desirable in applying an automatic control. Furthermore, it provides the system with simpler circuits than its counterparts [23].

From above mentioned, this paper proposes the application of CFTA and its modified-version, MO-CFTA, to generate the level shifted multicarrier PWM. The feature of the proposed circuit which is very simple consists of two MO-CFTAs, four CFTAs and one grounded capacitor. Moreover, the output signals are independent of temperature. This paper is organized as the following sections. Section 2 presents basic concept of MO-CFTA, saturation-mode on MO-CFTA, triangular carrier generation, comparator and principle of the proposed level shifted multicarrier PWM configuration. Section 4 shows the simulation results by PSpice program. In Section 5, the conclusion is presented.

2. Level Shifted Multicarrier PWM Circuit Design

In this section, we present the basic concepts of MO-CFTA for triangular carrier generation and CFTA for signal comparator. While, the circuit design for the proposed level shifted PWM will be presented in the last subsection 2.6.

2.1 Basic Concept of MO-CFTA

Fig. 4(a) shows the symbol of MO-CFTA that consists of nine-port analog and two ports for current bias. While Fig. 4(b) shows its equivalent circuit.

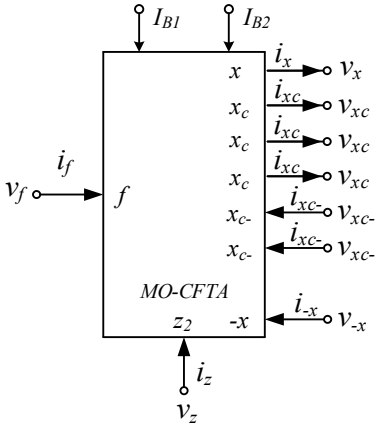

(a) Symbol

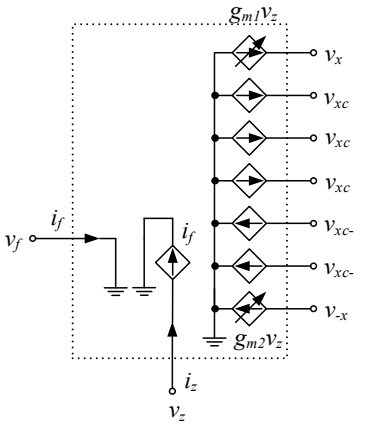

(b) Equivalent circuit

Fig. 4. Basic concept of MO-CFTA.

In an ideal case, the relationship between current and voltage can be found to be

$$\begin{bmatrix} V_f \\ I_z \\ I_x \\ I_{-x} \end{bmatrix} = \begin{bmatrix} 0 & 0 & 0 & 0 \\ 1 & 0 & 0 & 0 \\ 0 & g_{m1} & 0 & 0 \\ 0 & g_{m2} & 0 & 0 \end{bmatrix} \begin{bmatrix} I_f \\ V_z \\ V_x \\ V_{-x} \end{bmatrix}, \tag{1}$$

where
$$I_{xc} = I_x, I_{xc-} = -I_x, \tag{2}$$

and
$$g_{m1} = \frac{I_{B1}}{2V_T}, g_{m2} = \frac{I_{B2}}{2V_T} \tag{3}$$

where g_{m1} and g_{m2} are the transconductance gain of the MO-CFTA based on BJT technology, V_T is the thermal voltage and is equal to 26 mV at $27°C$, and I_{B1} and I_{B2} are bias currents used to adjust transconductance gain.

2.2 Saturation-Mode on MO-CFTA

From the MO-CFTA properties depicted in Section 2.1, when $V_Z << 2V_T$, the output currents at x (I_x) and $-x$ (I_{-x}) ports are equal to $V_Z I_{B1}/(2V_T)$ and $V_Z I_{B2}/(2V_T)$, respectively. The DC transfer characteristics of MO-CFTA can be approximated by the first order Taylor's series expansion [15], which can be explained as:

$$\tanh x = x - \frac{1}{3}x^3 + \frac{2}{15}x^5 - \frac{17}{315}x^7 + \ldots . \tag{4}$$

Thus, the original I_x and I_{-x} can be found by

$$I_x = I_{B1}\tanh\left(\frac{V_z}{2V_T}\right),\ I_{-x} = I_{B2}\tanh\left(\frac{V_z}{2V_T}\right). \tag{5}$$

Because the z port is floated, therefore, the output voltage at the z port can be approximated:

$$V_Z \approx \begin{cases} V_{CC} \text{ if } I_f \geq 0 \\ V_{EE} \text{ if } I_f \leq 0 \end{cases} \tag{6}$$

where V_{CC} and V_{EE} are the positive and negative supply voltages, respectively. From (6), it can be clearly seen that $V_Z >> 2V_T$. Then $\tanh(V_Z/(2V_T))$ in (4) and (5) can be approximately simplified to be

$$\tanh\left(\frac{V_z}{2V_T}\right) \approx 1 . \tag{7}$$

The condition of the MO-CFTA operates in the saturation-mode when $V_Z >> 2V_T$. Thus the output currents at x and $-x$ terminals can be re-written from (4) and (5) to be

$$I_x = \begin{cases} I_{B1} \text{ for } I_f \geq 0 \text{ when } V_Z >> 2V_T \\ -I_{B1} \text{ for } I_f \leq 0 \text{ when } V_Z >> 2V_T \end{cases} \tag{8}$$

and

$$I_{-x} = \begin{cases} I_{B2} \text{ for } I_f \geq 0 \text{ when } V_Z >> 2V_T \\ -I_{B2} \text{ for } I_f \leq 0 \text{ when } V_Z >> 2V_T \end{cases} \tag{9}$$

2.3 Current-Mode Multiple-Output Triangular Carrier Generation

The block diagram of the current-mode multiple-output triangular generation which is employed in the proposed circuit is shown in Fig. 5. It consists of two MO-CFTAs and one grounded capacitor. The MO-CFTA1 and MO-CFTA2 perform to be Schmitt trigger and integrator, respectively. The triangular-wave outputs can be generated via the alternately discharging and charging of capacitor which is demonstrated in Fig. 6.

From the properties of MO-CFTA as described in Section 2.1 and 2.2, I_{-x2} can be found to be

$$I_{-x2} = g_{m4}V_{z2} . \tag{10}$$

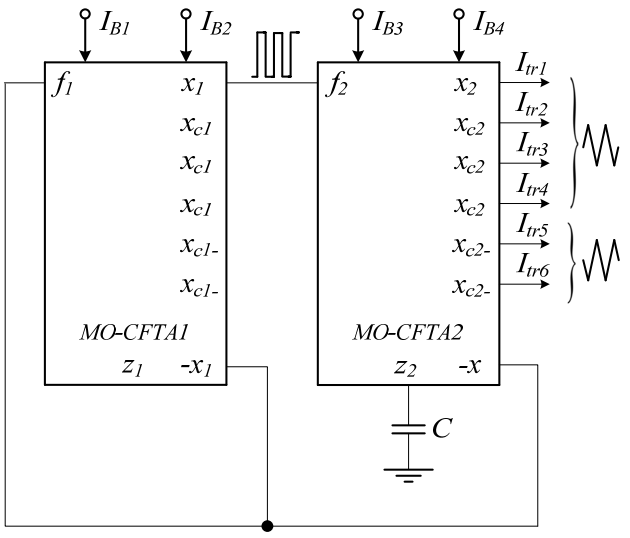

Fig. 5. Multiple-output triangular generation.

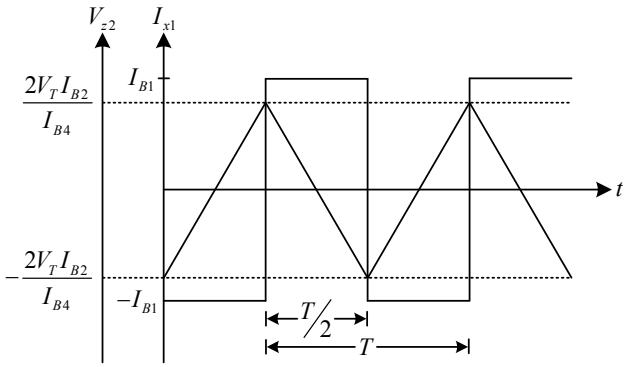

Fig. 6. Output waveforms of the multiple-output triangular generation.

Thus V_{z2} can be expressed to be

$$V_{z2} = \frac{I_{-x2}}{g_{m4}} = \frac{2V_T I_{-x2}}{I_{B4}} . \tag{11}$$

The amplitude of outputs $(I_{tr1} - I_{tr6})$ can be obtain by

$$I_{tr1} = I_{tr2} = I_{tr3} = I_{tr4} = g_{m3}V_{z2} = \frac{I_{B3}V_{z2}}{2V_T} \tag{12}$$

and

$$I_{tr5} = I_{tr6} = -g_{m3}V_{z2} = -\frac{I_{B3}V_{z2}}{2V_T} . \tag{13}$$

From (11), (12)-(13) can be rewritten as

$$I_{tr1} = I_{tr2} = I_{tr3} = I_{tr4} = \frac{I_{-x2}I_{B3}}{I_{B4}} \tag{14}$$

and

$$I_{tr5} = I_{tr6} = -\frac{I_{-x2}I_{B3}}{I_{B4}} . \tag{15}$$

From the DC characteristic of MO-CFTA explained in Section 2.1, it can be found that I_{-x2} depends on I_{B1}. Then $I_{tr1} - I_{tr6}$ can be ultimately written to be

$$I_{tr1} = I_{tr2} = I_{tr3} = I_{tr4} = \frac{I_{B1} I_{B3}}{I_{B4}} \tag{16}$$

and

$$I_{tr5} = I_{tr6} = -\frac{I_{B1} I_{B3}}{I_{B4}} \ . \tag{17}$$

Period T and output frequency can obtained by

$$T = 2 \int_{-V_{z2}}^{V_{z2}} \frac{C}{I_{B1}} dV_{z2} = \frac{8CI_{B2}V_T}{I_{B1}I_{B4}} \tag{18}$$

and

$$f = \frac{1}{T} = \frac{I_{B1}I_{B4}}{8CI_{B2}V_T} . \tag{19}$$

From (16), (17) and (19), it can be clearly seen that the magnitude and frequency of the output current can be electronically/independently controlled. In addition, the amplitude of output currents is free from V_T. Furthermore, the multiple-output triangular carrier generation is very suitable for applying in the multicarrier PWM more than another research option [24-37] which merely have a single output.

2.4 Current-Mode Comparator

Fig. 7 shows the block diagram of the current-mode comparator. The triangular carrier, I_{C1}, is subtracted from the information signal, i_i. Its result is sent to be an input of the comparator circuit. Equation (20) shows the condition of the output current of the comparator circuit, which can be explained by Fig. 8.

$$I_{O1} = \begin{cases} I_{B5} & \text{if } I_{C1} \le i_i \\ -I_{B5} & \text{if } I_{C1} \ge i_i \end{cases} \tag{20}$$

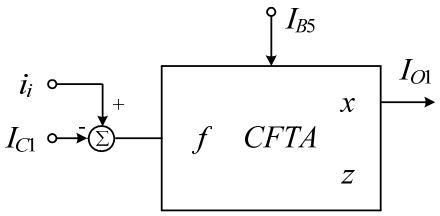

Fig. 7. Current-mode comparator (in case comparator 1).

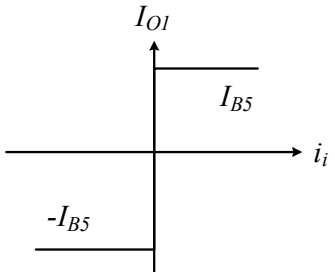

Fig. 8. DC characteristic of the current-mode comparator.

2.5 Current-Mode PWM Process

In this subsection, we explain the current mode PWM process. Fig. 9 shows the PWM signal that is generated by triangular carrier comparing with information signal. When the amplitude of triangular carrier is higher than that of information signal this produces the negative PWM signal, T_1, which can be found as following:

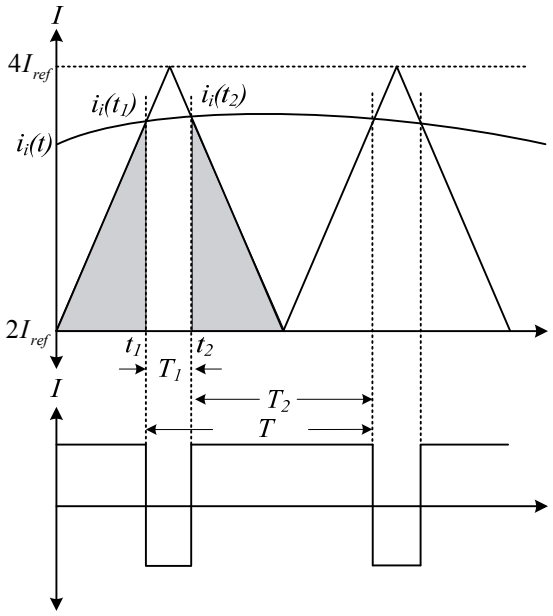

Fig. 9. Output waveforms of the proposed PWM (in case I_{O1}).

The slope of I_{C1} (m_{C1}), t_1 and t_2 can be found to be

$$m_{C1} = \frac{I_{B1}^2 I_{B3}}{2CV_T I_{B2}} \ , \tag{21}$$

$$t_1 = \frac{1}{m_{C1}} \int_{2I_{ref}}^{i_i(t_1)} dI_{C1} = \frac{I_{B1}^2 I_{B3}}{2CV_T I_{B2}} \left[i_i(t_1) - 2I_{ref} \right] \tag{22}$$

and

$$t_2 = -\frac{1}{m_{C1}} \int_{i_i(t_2)}^{2I_{ref}} dI_{C1} = -\frac{I_{B1}^2 I_{B3}}{2CV_T I_{B2}} \left[2I_{ref} - i_i(t_2) \right] \ . \tag{23}$$

From Fig. 9 and (22)-(23), T_1 can be expressed as

$$T_1 = T - (t_1 + t_2) = \frac{2CV_T I_{B2}}{I_{B1}} \left\{ \frac{4}{I_{B4}} - \frac{\left[\begin{matrix} i_i(t_1) \\ +i_i(t_2) \end{matrix} \right] - 4I_{ref}}{I_{B1}I_{B3}} \right\} . \tag{24}$$

From the piecewise linear approximation and the high frequency carrier signal $i_i(t_1) + i_i(t_2) \approx 2i_i(t)$. Thus (24) can be modified to be

$$T_1 = \frac{4CV_T I_{B2}}{I_{B1}} \left[\frac{2}{I_{B4}} - \frac{i_i(t) - 2I_{ref}}{I_{B1}I_{B3}} \right] . \tag{25}$$

Thereby, the duty cycle of I_{O1} can be obtained by

$$D_1 = \frac{T_1}{T} \times 100 = \frac{1}{2}\left\{2 - \frac{I_{B4}\left[i_i(t) - 2I_{ref}\right]}{I_{B1}I_{B3}}\right\} \times 100. \quad (26)$$

Similarly, the duty cycle of I_{O2}, I_{O3}, and I_{O4} can be found to be

$$D_2 = \frac{1}{2}\left[2 - \frac{I_{B4}i_i(t)}{I_{B1}I_{B3}}\right] \times 100, \quad (27)$$

$$D_3 = \frac{1}{2}\left[2 + \frac{I_{B4}i_i(t)}{I_{B1}I_{B3}}\right] \times 100, \quad (28)$$

and

$$D_4 = \frac{1}{2}\left\{2 + \frac{I_{B4}\left[i_i(t) - 2I_{ref}\right]}{I_{B1}I_{B3}}\right\} \times 100 \quad (29)$$

where D_1, D_2, D_3 and D_4 are duty cycle of I_{O1}, I_{O2}, I_{O3}, and I_{O4}, respectively.

From (26) and (29), if $i_i(t)$ is equal to $3I_{ref}$ and $-3I_{ref}$ resulting D_1 and D_4 are equal to 50% and if $i_i(t)$ is equal to I_{ref} resulting D_2 and D_3 are equal to 50%. While, if $I_{ref} = \frac{I_{B1}I_{B3}}{I_{B4}}$, equations (26) and (29) can be finally written as

$$D_1 = \frac{1}{2}\left[4 - \frac{I_{B4}i_i(t)}{I_{B1}I_{B3}}\right] \times 100 \quad (30)$$

and

$$D_4 = \frac{1}{2}\left[4 + \frac{I_{B4}i_i(t)}{I_{B1}I_{B3}}\right] \times 100. \quad (31)$$

From the properties of MO-CFTA and the operation of current-mode comparator described in Section 2.2 and Section 2.5, respectively, the amplitudes of I_{O2}, I_{O3}, and I_{O4} can be expressed as:

$$I_{O2} = \begin{cases} I_{B6} & \text{if } I_{C2} \le i_i \\ -I_{B6} & \text{if } I_{C2} \ge i_i \end{cases} \quad (32)$$

$$I_{O3} = \begin{cases} I_{B7} & \text{if } I_{C3} \le i_i \\ -I_{B7} & \text{if } I_{C3} \ge i_i \end{cases} \quad (33)$$

and

$$I_{O4} = \begin{cases} I_{B8} & \text{if } I_{C4} \le i_i \\ -I_{B8} & \text{if } I_{C4} \ge i_i \end{cases} \quad (34)$$

From (20) and (32)-(34), it can be found that the current level of I_{O1}, I_{O2}, I_{O3} and I_{O4} can be adjusted via bias currents. Furthermore, the amplitude of output currents is ideally temperature-insensitive by reason of liberty V_T.

2.6 Principle of the Proposed Level Shifted Multicarrier PWM

From the detail in Subsection 2.1-2.5, we use them to be information for designing the level shifted PWM circuit. Fig. 10 shows the block diagram of the proposed configuration. It consists of the multiple-output triangular carrier generation (circuit in Fig. 5) and four comparators (circuit in Fig. 7). Fig. 11, 12 and 13 illustrate the modulation process for PD, POD and APOD, respectively. From the process, they require the different DC level and phase of the triangular carrier signals. These requirements can be adjusted by I_{ref} and selecting the output ports of the circuit in Fig. 5, respectively.

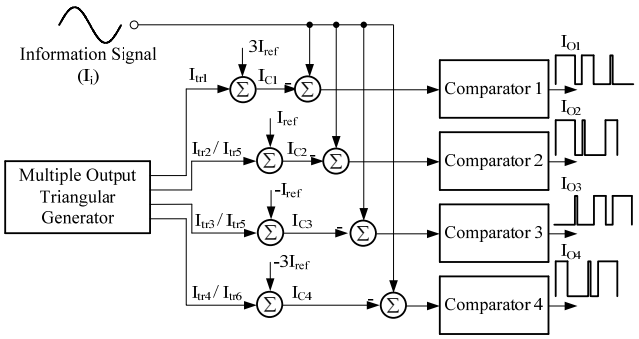

Fig. 10. Block diagram of the proposed level shifted multicarrier PWM.

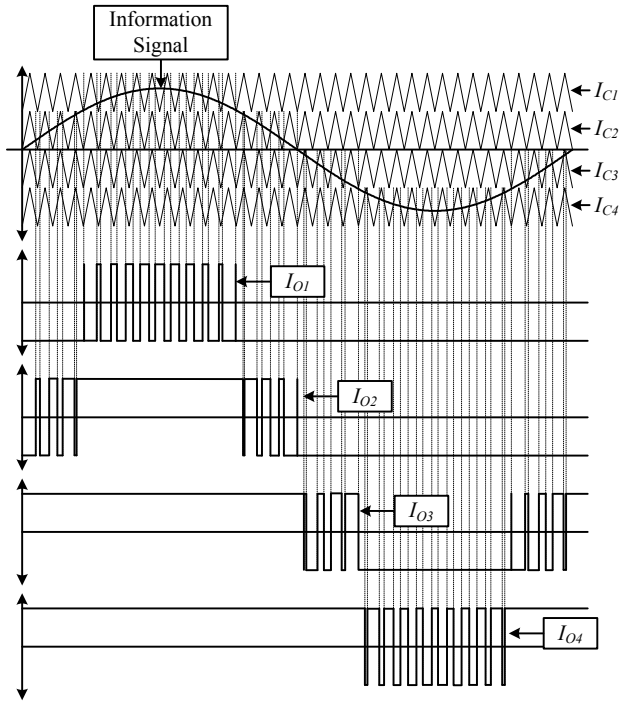

Fig. 11. Output waveforms of the PD level shifted multicarrier PWM.

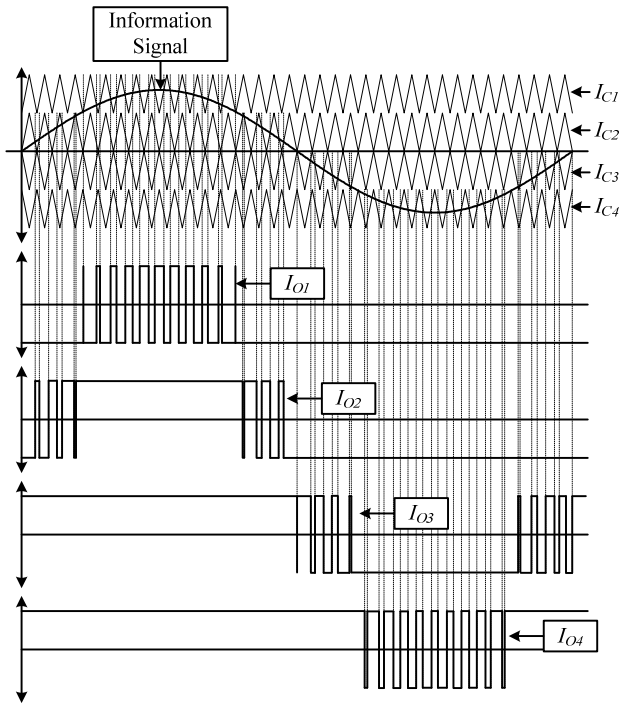

Fig. 12. Output waveforms of the POD level shifted multicarrier PWM.

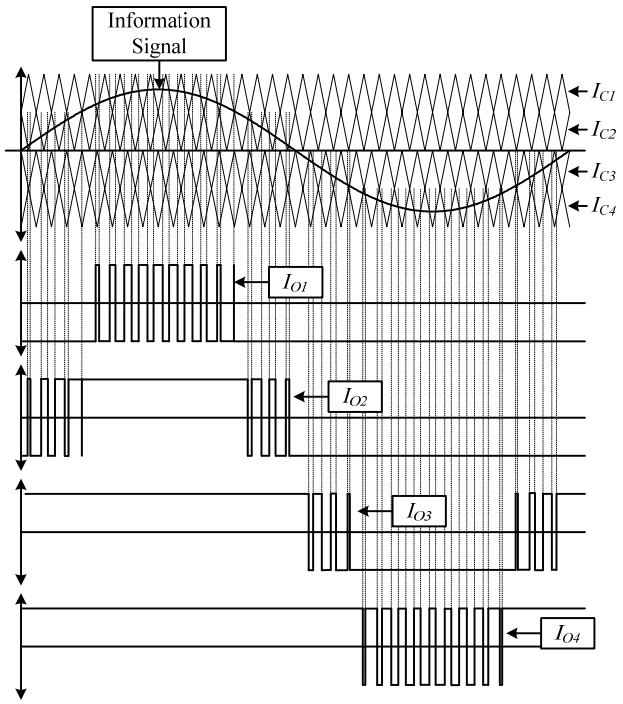

Fig. 13. Output waveforms of the APOD level shifted multicarrier PWM.

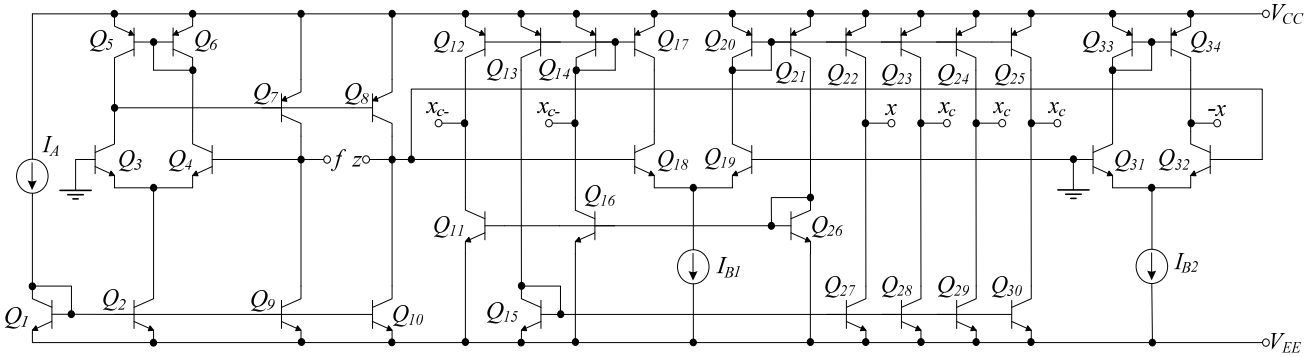

Fig. 14. Internal construction of MO-CFTA.

3. Simulation Result

The performances of the proposed level shifted multicarrier PWM have been confirmed via the simulation results by PSpice program. The schematic of MO-CFTA is shown in Fig. 14. The parameter of PNP and NPN transistors employed in the proposed circuit were simulated by using the parameters of the PR200N and NR200N bipolar transistors of ALA400 transistor array from AT&T [38]. DC power supply voltages are equal ±1.5 V, $C = 200$ nF, $I_A = 100$ μA, $I_{B1} = 100$ μA, $I_{B2} = 25$ μA, $I_{B3} = 95$ μA, $I_{B4} = 45$ μA, and $I_B = I_{B5} = I_{B6} = I_{B7} = I_{B8} = 100$ μA.

The simulation results in case of PD, POD and APOD are shown in Figs. 15-17. The output amplitude relative to the I_B variation is illustrated in Fig. 18. It can be clearly seen that the level of output current can be electronically adjusted by bias currents which are tuned from 0 to 800 μA.

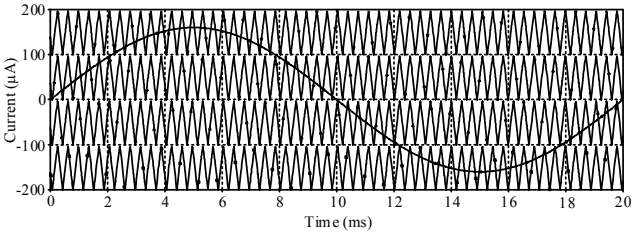

(a) Information signal and carrier signals.

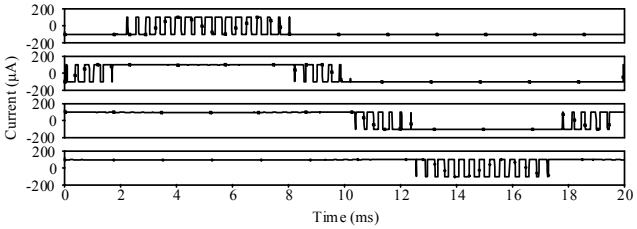

(b) The output signals.

Fig. 15. Results of the PD level shifted multicarrier PWM.

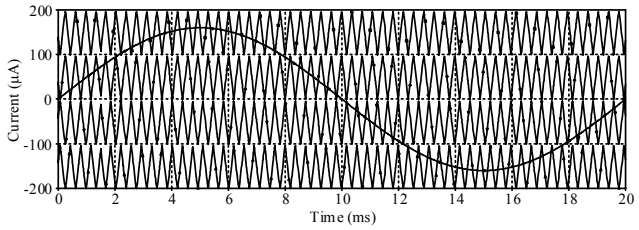

(a) Information signal and carrier signals.

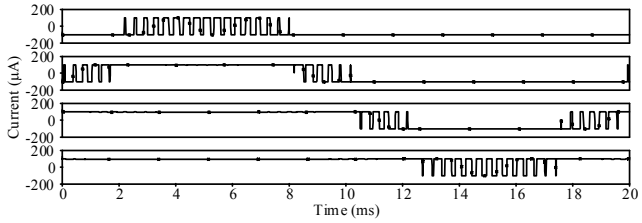

(b) The output signals.

Fig. 16. Results of the POD level shifted multicarrier PWM.

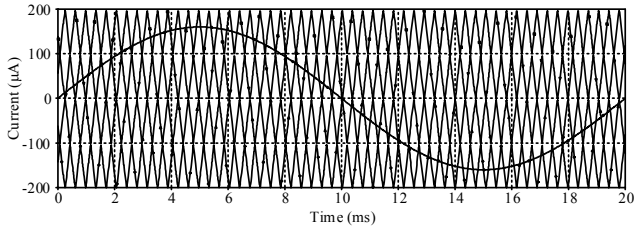

(a) Information signal and carrier signals.

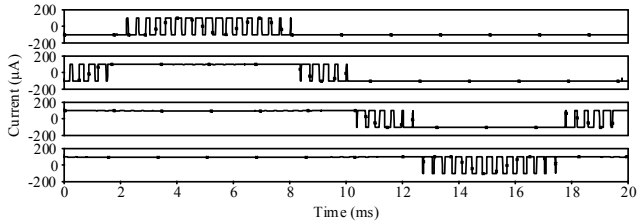

(b) The output signals.

Fig. 17. Results of the APOD level shifted multicarrier PWM.

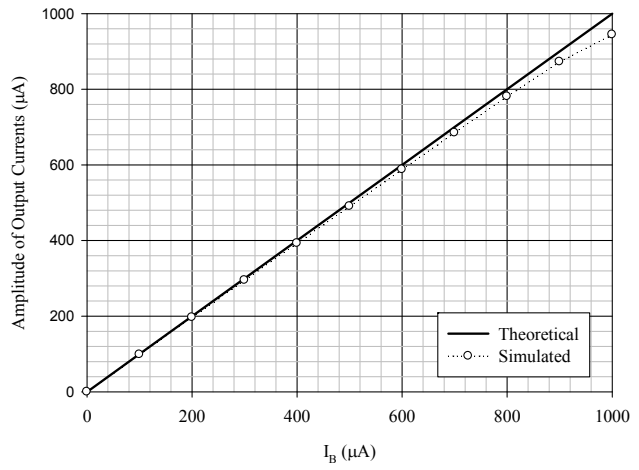

Fig. 18. Amplitude of output versus I_B.

The theoretical calculation and simulation of duty cycle is shown in Fig. 19. It can confirm that the results are in accordance with a theoretical analysis which is demonstrated in Section 2.6. The THD of the proposed PWM is approximately 2.68 % which is less than [16], [17], and [36].

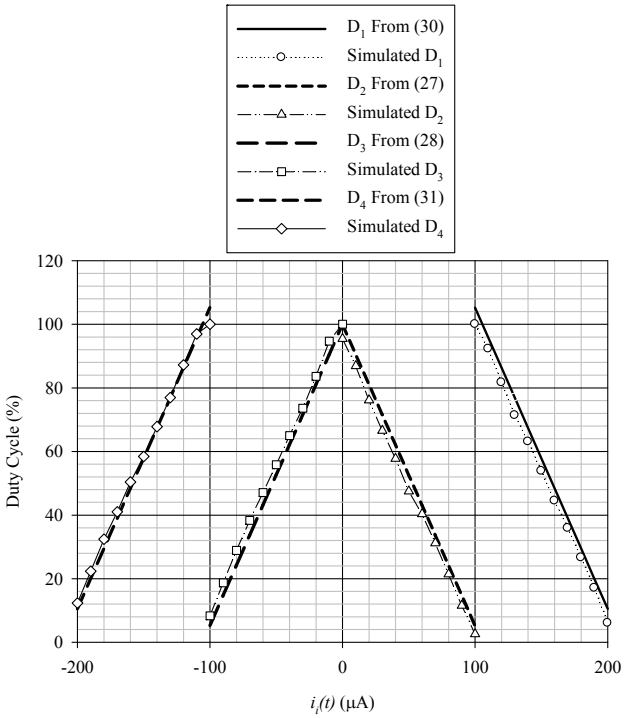

Fig. 19. Duty cycles against i_i(t).

The deviation of the output amplitude relative to temperature variation is demonstrated in Fig. 20. It can be found that the maximum absolute deviation of the level of output current is less than 1.37 % for temperature variation between 0 – 100°C. Therefore, it can be concluded that the amplitude of output currents is slightly dependent on wide temperature variation.

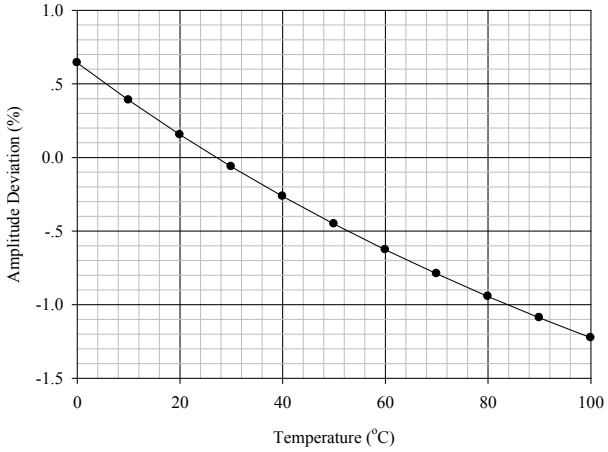

Fig. 20. Amplitude of PWM output versus temperature.

4. Conclusion

A novel current-mode PD, POD and APOD level shifted multicarrier is beneficial because the proposed

circuit comprises two MO-CFTAs, four CFTAs and a grounded capacitor without external resistor. The output current can be electronically controlled and is slightly dependent on wide temperature variation. The simulation results confirm that the theoretical expectation is possible. Moreover, this proposed circuit can be improved in further research which needs to use a multicarrier PWM application.

References

[1] RODRIGUEZ, J., LAI, J., PENG, F. Multilevel inverters: a survey of topologies, controls and applications. *IEEE Transaction on Industrial Application,* 2002, vol. 49, no. 4, p. 724-738.

[2] LESNICAR, A., MARQUARDT, R. An innovative modular multilevel converter topology suitable for a wide power range. In *Proceedings of Power Technology Conference*. 2003, vol.3, no. 6.

[3] ROSSMANN, W. C., ELLIS, R. G. Retrofit of 22 pipeline pumping stations with 3000-hp motors and variable-frequency. *IEEE Transactions on Industrial Application,* 1998, vol. 42, no. 1, p. 178 - 186.

[4] MENZ, R., OPPRECHT, F. Replacement of a wound rotor motor with an adjustable speed drive for a 1400 kW kiln exhaust gas fan. In *Proceedings of the 44th IEEE IAS Cement Industrial Technology Conference*. 2002, p. 85 - 92.

[5] SCHMITT, B. P., SOMMER, R. Retrofit of fixed speed induction motors with medium voltage drive converters using NPC three-level inverter high voltage IGBT based topology. In *Proceedings of the IEEE International Symposium Industrial Electronics*, 2001, p. 746 - 751.

[6] DIXON, J., MORAN, L., RODRIGUEZ, R., DOMKE, E. Reactive power compensation technologies: State-of-the-art review. *Proceedings of the IEEE*, 2005, vol. 39, no. 12, p. 2144 - 2164.

[7] ALEPUZ, S., BUSQUETS-MONGE, S., BORDONAU, J., GAGO, J., GONZALEZ, D., BALCELLS, J. Interfacing renewable energy sources to the utility grid using a three-level inverter. *IEEE Transactions on Industrial Electronics,* 2006, vol. 53, no. 5, p. 1504 - 1511.

[8] BERNERT, S. Recent development of high power converters for industry and traction applications. *IEEE Transactions on Industrial Electronics,* 2000, vol. 15, no. 6, p. 1102 - 1117.

[9] RODRIGUEZ, J., BERNET, S., WU, B., PONTT, J. O., KOURO, S. Multilevel voltage-source-converter topologies for industrial medium-voltage drives. *IEEE Transactions on Industrial Electronics,* 2007, vol. 54, no. 6, p. 2930 - 2945.

[10] TOLBERT, L. M., HABETLER, T. G. Novel multilevel inverter carrier-based PWM method. *IEEE Transaction on Industrial Application*, 1999, vol. 35, no. 5, p. 1098-1107.

[11] RADAN, A., SHAHIRINIA, A. H., FALAHI, M. Evaluation of carrier-based PWM methods for multi-level inverters. In *IEEE International Symposium on Industrial Electronics (ISIE)*. 2007, p. 389-394.

[12] SINGH, M., AGARWAL, A., KAIRA, N. Performance evaluation of multilevel inverter with advance PWM control techniques. In *IEEE 5th India International Conference on Power Electronics (IICPE)*. 2012, p. 1-6.

[13] CARRARA, G., GARDELLA, S., MARCHESONI, M., SALUTARI, R., SCIUTTO, G. A new multilevel PWM method: a theoretical analysis. *IEEE Transactions on Power Electronics*, 1992, p. 497-505.

[14] TOUMZOU, C., LIDEGY, F. J., HAIGH, D. *Analog IC Design: the Current-mode Approach*. Exeter (UK): Peter Peregrinus, 1990.

[15] SILAPAN, P., SIRIPRUCHYANUN, M. Fully and electronically controllable current-mode Schmitt triggers employing only single MO-CCCDTA and their applications. *Analog Integrated Circuits and Signal Processing*, 2011, vol. 68, no. 1, p. 111-128.

[16] KOOMBUN, J., SILAPAN, P., SIRIPRUCHYANUN, M. A fully electronically controllable current-mode derivative PWM signal generator employing MO-CTTAs. In *Proceedings of the 7th International Conference on Electrical Engineering/Electronics, Computer, Telecommunications, and Information Technology (ECTI-CON 2010)*. Chiang Mai (Thailand), 2010, p. 426-430.

[17] SRISAKUL, T., SILAPAN, P., SIRIPRUCHYANUN, M. An electronically controlled current-mode triangular/square wave generator employing MO-CCCCTAs. In *Proceedings of the 8th International Conference on Electrical Engineering/Electronics, Computer, Telecommunications, and Information Technology (ECTI-CON 2011)*. Khonkhen (Thailand), 2011, p. 82-85, 17-19.

[18] SIRIPRUCHYANUN, M., JAIKLA, W. Current-mode biquadratic filter using DO-CCCDBAs. *International Journal of Circuit Theory and Applications*, 2008, vol. 38, no. 3, p. 321–330.

[19] JAIKLA, W., NOPPAKARN, A., LAWANWISUT, S. New gain controllable resistor-less current-mode first order allpass filter and its application. *Radioengineering*, 2012, vol. 21, no. 1, p. 312–316.

[20] JAIKLA, W., SIRIPONGDEE, S., SUWANJAN, P. MISO current-mode biquad filter with independent control of pole frequency and quality factor. *Radioengineering*, 2012, vol. 21, no. 3, p. 886 to 891.

[21] JAIKLA, W., KHATEB, F., SIRIPONGDEE, S., SUWANJAN, P., SUPAVARASUWAT, P. Electronically tunable current-mode biquad filter employing CCCDTAs and grounded capacitors with low input and high output impedance. *International Journal of Electronics and Communications (AEU)*, 2013.

[22] HERENCSAR, N., KOTON, J., VRBA, K., LATTENBERG, I. Current follower transconductance amplifier (CFTA) - a useful building block for analog signal processing. *Journal of Active and Passive Electronic Devices,* 2011, vol. 1, no. 6, p. 217–229.

[23] BIOLEK, D., SENANI, R., BIOLKOVA, V., KOLKA, Z. Active elements for analog signal processing: classification, review, and new proposals. *Radioengineering*, 2008, vol. 17, no. 4, p. 15–32.

[24] SOTNER, R., SLEZAK, J., PETRZELA, J. Current mode tunable KHN filter based on controlled MO-CFTAs. *In 3rd International Conference on Signals, Circuits and Systems SCS2009*. Djerba (Tunis), 2009. p. 521-524.

[25] DE-MARCELLIS, A., DI-CARLO, C., FERRI, G., STORNELLI, V. A CCII-based wide frequency range square waveform generator. *International Journal of Circuit Theory and Applications*, 2013, vol. 41, no. 1, p. 1-13.

[26] CHIEN, H-CH. Voltage-controlled dual slope operation square/ triangular wave generator and its application as a dual mode operation pulse width modulator employing differential voltage current conveyors. *Microelectronics Journal*, 2012, vol. 43, no. 12, p. 962-974.

[27] ALMASHARY, B., ALHOKAIL, H. Current-mode triangular wave generator using CCIIs. *Microelectronics Journal*, 2000, vol. 31, no. 4, p. 239-243.

[28] PAL, D., SRINIVASULU, B. B., PAL, A., DEMOSTHENOUS, B., DAS, N. Current conveyor-based square/triangular waveform generators with improved linearity. *IEEE Transaction on Instrumentation and Measurement*, 2009, vol. 58, no. 7, p. 2174-2180.

[29] SAQUE, A. S., HOSSAIN, M. M., DAVIS, W. A., RUSSELL, H. T., CARTER, R. L. Design of sinusoidal, triangular, and square wave generator using current feedback amplifier (CFOA). In *Proc. of IEEE Region 5 Conference*. Kansas City (USA), 2008, p. 1–5.

[30] MINAEI, S., YUCE, E. A simple Schmitt trigger circuit with grounded passive elements and its application to square/triangular wave generator. *Circuits, Systems, and Signal Processing*, 2012, vol. 31, no. 3, p. 877-888.

[31] LO, Y. K., CHIEN, H. C. Switch-controllable OTRA-based square/triangular waveform generator. *IEEE Trans. on Circ. Syst. and Signal Processing II*, 2007, vol. 54, no. 12, p. 1110-1114.

[32] KIM, K., CHA, H. W., CHUNG, W. S. OTA-R Schmidtt trigger with independently controllable threshold and output voltage levels. *Electronics Letters*, 1997, vol. 33, no. 13, p. 1103-1105.

[33] CHUNG, W. S., KIM, H., CHA, H. W., KIM, H. J. Triangular/square-wave generator with independently controllable frequency and amplitude. *IEEE Transactions on Instrumentation and Measurement*, 2005, vol. 54, no. 1, p. 105-109.

[34] CHUNG, W. S., CHA, H. W., KIM, H. J. Current-controllable monostable multivibrator using OTAs. *IEEE Trans. on Circuits and Systems I*, 2002, vol. 49, no. 5, p. 703-705.

[35] SIRIPRUCHYANUN, M., WARDKEIN, P. A full independently adjustable, integrable simple current controlled oscillator and derivative PWM signal generator. *IEICE Trans. Fundam. Electron. Commun. Comput. Sci.*, 2003, vol. E86-A, no. 12, p. 3119-3126.

[36] KUMBUN, J., SIRIPRUCHYANUN, M. MO-CTTA-based electronically controlled current-mode square/triangular wave generator. In *Proc. of the 1st International Conf. on Technical Education (ICTE2009)*. 2010, p. 158–162.

[37] SOTNER, R., JERABEK, J., HERENCSAR, N., PROKOP, R., VRBA, K., PETRZELA, J., DOSTAL, T. Simply adjustable triangular and square wave generator employing controlled gain current and differential voltage amplifier. In *Proc. of the 23th Int.. Conf. Radioelektronika*. Pardubice (Czech Rep.), 2013, p. 111-116.

[38] FREY, D. R. Log-domain filtering: an approach to current-mode filtering. *IEE Proc. Circuit Devices Syst.*, 1993, vol. 140, p. 406 to 416.

About Authors …

Weerapon KONGNUN was born in Uttaradit, Thailand in 1976. He received the B. Eng. degree in Instrument Engineering and the M. Eng. degree in Electrical Engineering from King Mongkut's Institute of Technology Ladkrabang (KMITL) in 1999 and 2002. He was a lecturer at the Department of Electrical Computer and Industrial, Faculty of Industrial Technology, Uttaradit Rajabhat University, Uttaradit, Thailand since 2004. His research interests include electrical measurement, high voltage testing, power electronics and its application.

Apinan AURASOPON was born in Amnat-charoen Province, Thailand in 1971. He received his B.Eng in Electronic Engineering from Northeastern College in 1995, M.Eng. and Ph.D. in Electrical Engineering from King Mongkut's University of Technology Thonburi in 2003 and 2007, respectively. He was a lecturer at the Department of Electrical Engineering, Faculty of Engineering, Burapha University (BU), Chonburi in 2007 and transferred to the Faculty of Engineering, Mahasarakham University (MSU) in 2008, where he is Assistant Professor. His research interests include soft-switched converters, ac choppers, converter systems for improving power quality, and applying electronics and computer for agriculture.